Published in final edited form as:
Nanoscale. 2013 June 7; 5(11): 4944–4950. doi:10.1039/c3nr00290j.

Ratiometric Temperature Imaging Using Environment-Insensitive Luminescence of Mn-Doped Core/Shell Nanocrystals

Yerok Park[a], **Chiwan Koo**[b], **Hsiang-Yun Chen**[a], **Arum Han**[b,c], and **Dong Hee Son**[*,a]

[a]Department of Chemistry, Texas A&M University, College Station, Texas 77842, United States

[b]Department of Biomedical Engineering, Texas A&M University, College Station, Texas 77843, United States

[c]Department of Electrical and Computer Engineering, Texas A&M University, College Station, Texas 77843, United States

Abstract

We report a ratiometric temperature imaging method based on Mn luminescence from Mn-doped CdS/ZnS nanocrystals (NCs) with controlled doping location, which is designed to exhibit strong temperature dependence of the spectral lineshape while being insensitive to the surrounding chemical environment. Ratiometric thermometry on Mn luminescence spectrum was performed by using Mn-doped CdS/ZnS core/shell NCs that have a large local lattice strain on Mn site, which results in the enhanced temperature dependence of the bandwidth and peak position. Mn luminescence spectral lineshape is highly robust with respect to the change in the polarity, phase and pH of the surrounding medium and aggregation of the NCs, showing great potential in temperature imaging under chemically heterogeneous environment. The temperature sensitivity ($\Delta I_R/I_R$ = 0.5%/K at 293 K, I_R = intensity ratio at two different wavelengths) is highly linear in a wide range of temperatures from cryogenic to above-ambient temperatures. We demonstrate the surface temperature imaging of a cyro-cooling device showing the temperature variation of >200 K by imaging the luminescence of the NC film formed by simple spin coating, taking advantage of the environment-insensitive luminescence.

Keywords

Nanothermometer; doped semiconducting nanocrystals; ratiometric temperature sensing; environment-insensitive luminescence

1. Introduction

Recent progress in luminescence thermometry using temperature-dependent luminescence of various molecular and nanocrystalline materials made it possible to measure the temperature optically with high accuracy (<0.1 °C) and spatial resolution (<10 μm).[1–12] The luminescence thermometry has been applied to the temperature sensing of various platforms such as micro/nanofluidics, integrated devices and intracellular environment.[13–18]

[*] Tel: 979-458-2976; dhson@mail.chem.tamu.edu.

[†]Electronic Supplementary Information (ESI): Synthesis details and TEM images of Mn-doped nanocrystals are available via DOI: 10.1039/b000000x/

Temperature dependence of the intensity, spectral position, bandwidth, polarization and lifetime of the luminescence are among the frequently utilized temperature sensing mechanisms in luminescence thermometry.[3–6] Therefore, the insensitivity of these characteristics of luminescence to the other variables besides the temperature is very important for the accurate and reliable temperature sensing.[16, 19, 20] However, the luminescence of many materials utilized for temperature sensing is often affected by the variation of the surrounding chemical environment at a given temperature. For instance, luminescence intensity and peak position of many thermo-sensitive dye molecules vary significantly as the polarity or pH of the surrounding medium changes.[19, 21] The lifetime of the luminescence can also be influenced by the surrounding medium interfering with the temperature measurement.[2, 22] In the case of quantum dots, the variation of the surface functionalization and interparticle distance can change the exciton luminescence intensity and spectrum.[23–25]

One strategy that was shown to be effective in reducing the environmental sensitivity of the luminescence thermometry is to coat the temperature-sensing material with `shell' material that forms a barrier between the sensor and the surrounding medium. For instance, a thick polymer layer formed on the thermosensitive fluorescent dye-imbedded nanoparticles effectively reduced the sensitivity of the luminescence lifetime to the variation of pH and ionic strength, enabling more reliable temperature sensing.[26] In the case of the thermometry based on the luminescence intensity, ratiometric measurement of the multiple emitters has become more common recently, where the temperature-dependent ratio of the two different luminescence intensities is measured instead of the absolute intensity. The dual emitting materials used for such purpose include lanthanide-codoped nanoparticles or metal-organic framework (two dopant emissions) and Mn-doped quantum dot (exciton and dopant emissions).[7–11] Since the intensity ratio fluctuates much less than the absolute intensity, the ratiometric thermometry is generally more accurate than non-ratiometric methods for the optical temperature imaging.

While the ratiometry allows more robust intensity-based luminescence thermometry, the environmental sensitivity still remains as a challenging issue due to the potentially unequal effect of the surrounding environment on the intensities of the different emitters. For instance, the luminescence intensities of exciton and dopant in nanocrystals are affected differently by the charge carrier-accepting molecules (e.g., thiols) or the dissolved oxygen present in the surrounding medium depending on the spatial proximity of the emitter and the molecules affecting the luminescence.[27, 28]

Here, the ratiometric surface-temperature imaging of a cryo-cooling device in a wide temperature range (77– 260 K) is demonstrated by using Mn luminescence from Mn-doped CdS/ZnS core/shell nanocrystals with controlled host structure and doping location, which is highly insensitive to the surrounding chemical environment and exhibits near-linear temperature response in a broad range of temperatures (100 – 380 K). The diminished sensitivity of the method reported here to the environmental variation is ascribed to the use of `single' luminescence from Mn^{2+} ions doped far below the surface of the nanocrystals (~2.1 nm) with controlled doping radius, whose spectral lineshape is highly insensitive to the environment outside of the nanocrystals. For the same reason, high quantum yield of luminescence can be maintained even under the conditions that are known to significantly diminish the exciton luminescence. The broad bandwidth (~90 nm at 293 K) and robust Mn luminescence spectrum enable the ratiometric thermometry even with a single luminescing species, i.e., Mn^{2+} ions. The temperature sensitivity ($\Delta I_R/I_R$ = ~0.5%/K at 293 K, I_R = intensity ratio) in a wide range of temperatures was obtained by controlling the local lattice strain at the dopant site, which significantly enhances the bandwidth broadening and peak shift with temperature increase.[29, 30] Since only a single emitting species is used, the issue

of potentially different effect of the surrounding environment on different emitters is avoided. Here, we performed the ratiometric surface temperature imaging of a glass substrate partially exposed to the liquid nitrogen to demonstrate the capability of the reliable thermometer in a wide range of temperatures. Despite the inhomogeneity of the nanocrystal coating formed on the substrate via spin coating, the surface temperature ranging from 77 to 260 K could be reliably imaged on a CCD camera thanks to the environmental insensitivity of Mn luminescence and large dynamic range of temperature sensing. The ratiometric temperature imaging with Mn-doped CdS/ZnS nanocrystals demonstrated in this study will be particularly useful for the optical surface-temperature imaging of the chemically heterogeneous system with a large distribution of temperatures.

2. Experimental

2.1 Synthesis of Mn-doped CdZ/ZnS core/shell nanocrystals (NCs) with controlled radial doping location

Mn-doped CdS/ZnS core/shell NCs with controlled radial doping location and doping concentration were synthesized employing SILAR (Successive Ionic Layer Adsorption and Reaction) method previously reported.[31–33] The key control in the synthesis of Mn-doped CdS/ZnS core/shell NCs used in this study is the radial doping location of Mn^{2+} ions within the core/shell host NCs with lattice mismatch, which determines both the temperature sensitivity of Mn luminescence and its insensitivity to the surrounding chemical environment as discussed in detail in Results and Discussions. CdS core (3.6 nm) was prepared by injecting 1-octadecene (ODE) solution of sulfur to the mixture of cadmium oxide, ODE, and oleic acid at 250 °C. ZnS shell was coated using SILAR method by introducing the precursors of anion and cation alternately. ODE solution of sulfur and toluene solution of zinc stearate were used as the precursor of S and Zn respectively. The radial Mn doping location was controlled by introducing Mn precursor at different steps during the layer-by-layer coating of ZnS shell. Oleylamine solution of Mn acetate or Mn diethyldithiocarbamate was used as the precursor of Mn. The details of the synthesis are provided in the Supporting Information.

2.2 Measurement of the temperature-dependent Mn luminescence spectra

Mn-doped CdS/ZnS NCs mixed with poly(methyl methacrylate) were spin-coated on the sapphire substrate. The temperature was controlled in an open-cycle cryostat (ST-100, Janis) using liquid nitrogen as the cryogen. The NCs on sapphire substrate were excited by a 403 nm *cw* diode laser at a low power (< 1 mW at 5 mm beam diameter). The luminescence spectra were measured with a fiber optic-coupled CCD spectrometer (QE65 Pro, Ocean Optics). A 450 nm long pass filter was used to block the scattered excitation light. The transmittance spectra of the two bandpass filters used for imaging (600 and 650 nm, 10 nm bandwidth) were used to obtain the temperature calibration curve from the measured Mn luminescence spectra.

2.3 Cryo-cooling device fabrication

Fig. 1(a) illustrates the construction of the cryo-cooling device that provides a temperature gradient from 77–260 K over ~12 mm distance. Thin film of Mn-doped NCs was formed on a glass substrate from the solution of the NCs dispersed in chloroform via spin-coating. On top of the NCs-coated glass substrate, 15 μm-thick poly(dimethylsiloxane) (PDMS) layer was spin-coated and cured. The black PDMS substrate having a channel for the liquid nitrogen ($3\times3\times10$ mm^3, w×h×l) was replicated from a polymer master mold fabricated using a 3D printer (ULTRA, envision TEC). Before applying the uncured black PDMS to the master mold, two silicon tubes were connected at the inlet and outlet port of the liquid nitrogen channel. The black PDMS was cured in an oven at 80 °C for 1 hour and

permanently bonded to the NCs-coated glass substrate. The device was placed in the enclosure made of black acetal resin blocks. The front of the enclosure has a glass window for the illumination and imaging purpose. The enclosure has the inlet and outlet port for the dry nitrogen gas used for flushing the interior of the enclosure.

2.4 Surface temperature imaging of the cyro-cooling device

The surface temperature profile of the cryo-cooling devices was measured with the setup shown in the Fig. 1(b). Liquid nitrogen flowing through the channel cooled the region of the glass substrate in contact with liquid nitrogen to 77 K. The dry nitrogen flow through the enclosure prevents frosting on the surface of the glass substrate and maintains the temperature gradient between 77 K and ambient temperature on the glass substrate. The cryo-cooling device was illuminated with a 365 nm UV LED and a collimating lens. 475 nm short-pass filter (F1) was placed after the LED to remove the red tail of the spectrum. A dichroic mirror (DMLP505R, Thorlabs) was used to reflect the excitation light from the LED and collect the luminescence from the device. A combination of an achromatic doublet lens (L2, focal length = 200 mm) and a microscope tube lens (L3, focal length = 200 mm) was used to image the surface of the device on the CCD camera (Princeton Instrument, PI-LCX) at 1X magnification. Temperature image was generated by taking the ratio of the two intensity images at 600 and 650 nm and using the calibration curve shown in Fig. 2(b). Each intensity image at 600 and 650 nm was separately recorded with 20 sec integration time by placing a bandpass filter (F3) in front of the CCD. With this setup, each pixel of CCD images $20\times20\ \mu m^2$ area.

2.5 Finite element method (FEM) simulation

To simulate the temperature profile at the interface of glass and PDMS of the cryo-cooling device, FEM models were implemented using Comsol Multiphysics™. Thermal conductivity parameters of 0.18 W mK^{-1} and 1.38 W mK^{-1} were selected for PDMS and glass, respectively. The temperature of the liquid nitrogen channel inside the PDMS block was set as 77 K. Outside boundary of the glass substrate had the heat flux with the heat transfer coefficient of 40 W $m^{-2}K^{-1}$. A forced convection was assumed to account for the dry nitrogen gas flow over the device.

2. Results and Discussions

Fig. 2(a) shows the luminescence spectra of Mn-doped CdS/ZnS core/shell nanocrystals (NCs) used in this study in the temperature range of 77 to 380 K. The Mn^{2+} ions are doped at the interface between the CdS core (3.6 nm in diameter) and the ZnS shell (2.1 nm in thickness) at the average doping concentration of ~45/particle determined from the elemental analysis. The two dashed curves in Fig. 2(a) are the transmittance spectra of the bandpass filters centred at 600 and 650 nm used for the ratiometric temperature imaging in this study. These two wavelengths are chosen since the ratio of the intensities exhibit a large usable linear dynamic and the simple bandpass filter can readily separate them spectrally. Fig. 2(b) shows the ratio of the intensities ($I_R = I_{600}/I_{650}$) measured with the two band-pass filters in the temperature range of 77–380 K normalized to the intensity ratio (I_R) at 293 K, which serves as the temperature calibration curve. Near the ambient temperature, $_IR$ varies at the rate of 0.5%/K.

The structure of the NCs used in this study was specifically controlled to enhance the temperature dependence of the bandwidth and peak position. Our recent study indicated that the local lattice strain at Mn^{2+} sites softens the vibrational mode coupled to Mn luminescence and increases local thermal expansion, which results in a significant enhancement of the bandwidth broadening and peak shift with the temperature increase.[30]

The local lattice strain arises from the lattice mismatch between the core and shell, which increases as it gets closer to the core/shell interface. In the NCs used in this study, the local lattice strain on Mn^{2+} ions was maximized by doping at CdS/ZnS interface employing SILAR (Successive Ionic Layer Adsorption And Reaction) method to maximize the temperature dependence of Mn luminescence. For comparison, significantly weaker temperature dependence of Mn luminescence spectra from Mn-doped NCs, where Mn^{2+} ions are doped at low-strain region in the ZnS shell, is shown in Fig. 2(c). Since the diffusion of Mn^{2+} ions within the host NC is negligible below <400 K, the structurally optimized temperature dependence of Mn luminescence spectrum is maintained robustly within the temperature range of our study. Above ~500K, however, the diffusion of Mn^{2+} ions begins to become non-negligible and limits the applicability at the higher temperatures.[34, 35]

In general, the ratiometric luminescence thermometry using the luminescence intensities of two emitting states is based on the Boltzmann population determined by $e^{\Delta E/kT}$, where ΔE is the energy difference between the two emitting species. In this work, while we rely on a single emitting species (i.e., Mn^{2+} ions), the situation is similar to having a multiple number of emitting states separated by the energy of the coupled vibrational mode, whose populations also follow the Boltzmann statistics. Because of the broadening of each vibronic transition that results in the smooth spectral lineshape, luminescence from higher-lying state appears as the broadening of the spectral lineshape.[30] In this sense, the temperature measurement based on Mn luminescence operates on the same principle as the typical ratiometric method based on multiple emitting species. The linear increase of Mn luminescence bandwidth above ~70 K follows the functional form of $\coth(\hbar\omega/2kT)$ and the linear local thermal expansion, where ω is the frequency of the vibrational mode coupled to Mn emission.[29, 30]

The potential influence of the surrounding environment on the luminescence is the common issue for the luminescence thermometry and poses a challenge in temperature sensing under the chemically heterogeneous environment such as in the biological cell.[16–18, 20, 26, 36, 37] For the fluorescence of the molecular species and the exciton fluorescence of quantum dots, both the intensity and the shape of the luminescence spectra can vary with the polarity of the surrounding medium or concentration of the fluorophore due to solvatochromism or interparticle electronic coupling.[21, 25, 38, 39] In the case of semiconductor quantum dot, the surfactant molecules can also influence the luminescence intensity via charge carrier transfer between the surfactant and the quantum dot to a varying degree depending on the structure of the quantum dot.[40] Therefore, the potential differences in the effect of the surrounding environment on the luminescence of the different emitting species can complicate even the ratiometric temperature sensing. A common strategy that has been used to address such issue is adding a thick shell (e.g., polymer) that surrounds the sensor material and prohibits the access of the molecules in the surrounding medium. In Mn-doped core/shell NCs used in this work, the inorganic shell (ZnS) combined with the local nature of the *d* electrons of Mn makes Mn luminescence highly insensitive to the surrounding medium even without thick polymer shell.

Fig. 3(a)–(c) exemplify the robustness of Mn luminescence spectrum with respect to the large variation of several environmental variables, such as the solvent polarity, surface-passivating molecules, concentration of the NCs and pH of aqueous medium. All the NCs used in the above comparison have ~2.1 nm of ZnS shell above Mn^{2+} ions and passivated with organic surfactants with aliphatic tail group containing 11–18 carbons. Fig. 3(a) compares the Mn luminescence spectra of the NCs at 293 K dispersed in chloroform and water that have very different polarity (ε = 4.8 vs. 80.4 for chloroform and water at 293 K respectively). The two NCs also have different surface-passivating surfactant to give the

solubility in each solvent, i.e., oleic acid and 11-mercaptoundecanoic acid (MUA) for chloroform and water respectively. The bottom panel shows the difference between the two normalized spectra (ΔI) in two different solvents. Even with such extreme difference in the solvent polarity and the surface passivating functional group, the two spectra are very close with less than 1% difference introduced to the value of ΔI (< 2 K shift in temperature). The difference of the spectra between the two different solvents with relatively small difference in polarities (e.g., hexane and toluene) is within the noise level of detection by the spectrometer.

Fig. 3(b) compares Mn luminescence spectra of the oleic acid-passivated NCs in different phases of the surrounding medium: liquid (chloroform), solid substrate in vacuum (sapphire) and polymer film on solid substrate (PMMA/sapphire). The sample on the sapphire was prepared by drop-casting the concentrated chloroform solution of NCs and forms an aggregate of the NCs. The sample in the polymer medium was prepared by spin coating the dilute NC solution in PMMA-chloroform mixture. The difference of the spectra (blue: s_1-s_3, red: s_1-s_4) shown in the bottom panel indicates less than 1% variation in ΔI is introduced by the change of phase of the surrounding medium and aggregation. The spectra from the aggregated NCs and dispersed NCs in PMMA polymer were nearly identical within the noise of the spectrometer. Fig. 3(c) shows the pH-dependent Mn luminescence spectrum of MUA-passivated NCs. Even with the onset of partial aggregation of the NCs at pH 5, the luminescence spectra remains highly robust with less than 0.5% change in ΔI. Compared to the materials with thick (tens of nm) polymer shell that has been used to protect the temperature sensing nanoparticles, inorganic core/shell structure can provide comparable protection at much smaller sizes. For Mn-doped CdS/ZnS NCs studied here, thickening of ZnS shell or adding the polymer shell is expected to further improve the insensitivity of the luminescence spectrum to the surrounding environment.

Having established the robustness of the temperature-dependent Mn luminescence spectral lineshape with respect to the variation of the surrounding environment, we performed imaging of the surface temperature of a cryo-cooling device experiencing a large thermal gradient. Fig. 4(a) shows the structure of the device, where the liquid nitrogen flows in the channel formed under the glass substrate by the black poly(dimethylsiloxane) (PDMS) polymer. Such device that provides local cryo-cooling has been used in low-temperature applications, e.g., cryo magnetic resonance imaging.[41] However, the spatially-resolved temperature profile at the interface of two materials in such device could not be measured readily. To measure the temperature distribution at the interface of the glass substrate and PDMS in this study, Mn-doped NCs were spin-coated on the side of the glass substrate facing the PDMS polymer.

Fig. 4(b) and 4(c) shows the color contour plot of the raw intensity profile at 650 nm (I_{650}) and the temperature profile obtained from I_R respectively. The color contour plot of the raw intensity profile at 600 nm (I_{600}) is presented in Fig. S2(a) in the Supporting Information. For this measurement, the steady flow of liquid nitrogen in the channel and constant flush of dry nitrogen gas at 293 K above the surface of the glass substrate were maintained as described in detail in the Experimental section. The ratiometric temperature imaging was performed using a CCD camera by taking the ratio of the two intensity images recorded at 600 and 650 nm. The intensity image at each wavelength was taken using the bandpass filter placed in front of the CCD with the exposure time of 20 sec. A UV LED that illuminates the area of ~5 cm^2 was used as the excitation source.

Despite the inhomogeneous NC coating and the uneven lighting condition by the LED, giving rise to a large spatial fluctuation in the absolute luminescence intensity, the measured temperature profile shows a very smooth variation. In Fig. 4(d), a line profile of the

temperature at a chosen location is shown. The temperature gradient from 77 to 260 K developed over the distance of 12 mm is clearly observed. The superimposed dashed line is the result of finite element method (FEM) calculation performed with a commercially available FEM software (Comsol Multiphysics™, COMSOL Inc.) described in the Experimental section.[41] In this simulation, the effect of dry nitrogen flushing over the device was accounted for by adjusting the value of the heat transfer coefficient (h) at the glass/nitrogen interface. Using the value of $h = 40$ that corresponds to the thermal conductivity of the glass under the highly convective environment, a good agreement between the calculated and measured temperature profile is obtained. The average noise in the temperature image shown in Fig. 4(c) is ±1 K, which is mainly due to the limitation of the imaging with a CCD camera, where different area is sensed by different pixels. However, the signal to noise ratio can be improved by averaging the multiple number of images from the CCD or employing scanning imaging technique combined with more sensitive detectors.

In order to test the stability and resolution of the temperature sensing based on Mn luminescence spectral lineshape, we measured the luminescence spectrum of a solution sample as a function of time with a CCD spectrometer instead of imaging with a CCD camera. Fig. 5 shows the temperature of the solution sample in a cuvette measured with the integration time of 10 msec at 10 sec interval. During the first 25 min, the temperature of the cuvette was kept constant. Subsequently, the temperature of the cuvette was increased by flowing warm nitrogen gas to the exterior of the cuvette. Heating of the cuvette was stopped after 5 min and the cuvette was allowed to return to the initial ambient temperature. The temperature change was detected with less than ±0.05 K of noise demonstrating the robustness and sensitivity of the temperature sensing method.

The key advantages of the temperature imaging method described here are the highly insensitive spectral lineshape of Mn luminescence with respect to the variation of the surrounding chemical environment and the wide linear dynamic range of temperature sensing. The temperature of chemically heterogeneous surface can be reliably imaged via spin coating or spraying of the NCs. High quantum yield of Mn-doped NCs used in this study (>35%), which is maintained even with particle aggregation and thiol passivation, is another advantage over other quantum dot-based temperature sensors. A broad measurable temperature range (ΔT ±300 K) extending from cryogenic to above-ambient temperature with a linear correlation between the temperature and the measured signal will be particularly suitable for the temperature imaging a large thermal gradient, such as the device with local heating or cooling. On the other hand, for the application requiring the higher temperature sensitivity in a narrower temperature range, such as in the living biological cells, the present method provides the relatively lower sensitivity in physiological temperature range (295–320K) compared to some of the reported results.[2] However, the sensitivity of the temperature measurement demonstrated in Fig. 5 may be sufficient for the biological temperature imaging with high temperature resolution as well as the other extreme requiring larger temperature coverage.

3. Conclusion

We report the ratiometric temperature imaging based on temperature-dependent Mn luminescence spectrum from Mn-doped CdS/ZnS NCs that is highly insensitive to the surrounding environment and exhibiting near-linear temperature response in a broad range of temperatures (100–380 K). The Mn luminescence from the NCs used in this study was made highly insensitive to the variation of the surrounding environment, such as the surface passivation, polarity and pH of medium, by confining Mn^{2+} ions below the shell in core/shell structure of the NC. The temperature sensitivity of the spectrum was enhanced by utilizing the local lattice strain created by the core/shell lattice mismatch that results in the

stronger bandwidth broadening and peak shift with the temperature increase. Taking advantage of the weak environmental sensitivity of Mn luminescence spectrum and large temperature sensing range, we demonstrate the ratiometric temperature imaging of a cryo-cooling device. The surface temperature profile of the device ranging from 77 to 260 K was readily imaged with a CCD camera from the luminescence of the NCs spin-coated on the surface of the substrate. The method shown here will be particularly useful for the temperature imaging of the surfaces exhibiting a wide range of temperature variation and exposed to the chemically inhomogeneous environment.

Supplementary Material

Refer to Web version on PubMed Central for supplementary material.

Acknowledgments

D.H.S. gratefully acknowledges the support from Welch Foundation (Grant No. A-1639). This work was partially supported by the National Institutes of Health/National Institute of Biomedical Imaging and Bioengineering (NIH/NIBIB) grant 1R21EB07297 to A.H.

Notes and references

1. Fischer LH, Harms GS, Wolfbeis OS. Angew. Chem. Int. Ed. 2011; 50:4546–4551.
2. Brites CDS, Lima PP, Silva NJO, Millan A, Amaral VS, Palacio F, Carlos LD. Nanoscale. 2012; 4:4799–4829. [PubMed: 22763389]
3. Jaque D, Vetrone F. Nanoscale. 2012; 4:4301–4326. [PubMed: 22751683]
4. Walker GW, Sundar VC, Rudzinski CM, Wun AW, Bawendi MG, Nocera DG. Appl. Phys. Lett. 2003; 83:3555–3557.
5. Uchiyama S, Matsumura Y, de Silva AP, Iwai K. Anal. Chem. 2003; 75:5926–5935. [PubMed: 14588034]
6. Liebsch G, Klimant I, Wolfbeis OS. Adv. Mater. 1999; 11:1296–1299.
7. Singh SK, Kumar K, Rai SB. Sens. Actuators, A. 2009; 149:16–20.
8. Brites CDS, Lima PP, Silva NJO, Millán A, Amaral VS, Palacio F, Carlos LD. Adv. Mater. 2010; 22:4499–4504. [PubMed: 20803765]
9. Cui Y, Xu H, Yue Y, Guo Z, Yu J, Chen Z, Gao J, Yang Y, Qian G, Chen B. J. Am. Chem. Soc. 2012; 134:3979–3982. [PubMed: 22352469]
10. Vlaskin VA, Janssen N, van Rijssel J, Beaulac R. m. Gamelin DR. Nano Lett. 2010; 10:3670–3674. [PubMed: 20704326]
11. Hsia C-H, Wuttig A, Yang H. ACS Nano. 2011; 5:9511–9522. [PubMed: 22032176]
12. Ye F, Wu C, Jin Y, Chan Y-H, Zhang X, Chiu DT. J. Am. Chem. Soc. 2011; 133:8146–8149. [PubMed: 21548583]
13. Mao H, Yang T, Cremer PS. J. Am. Chem. Soc. 2002; 124:4432–4435. [PubMed: 11960472]
14. Graham EM, Iwai K, Uchiyama S, Prasanna de Silva A, Magennis SW, Jones AC. Lab on a Chip. 2010; 10:1267–1273. [PubMed: 20445879]
15. Sadat S, Tan A, Chua YJ, Reddy P. Nano Lett. 2010; 10:2613–2617. [PubMed: 20550098]
16. Gota C, Okabe K, Funatsu T, Harada Y, Uchiyama S. J. Am. Chem. Soc. 2009; 131:2766–2767. [PubMed: 19199610]
17. Yang J-M, Yang H, Lin L. ACS Nano. 2011; 5:5067–5071. [PubMed: 21574616]
18. Okabe K, Inada N, Gota C, Harada Y, Funatsu T, Uchiyama S. Nat Commun. 2012; 3:705. [PubMed: 22426226]
19. Zohar O, Ikeda M, Shinagawa H, Inoue H, Nakamura H, Elbaum D, Alkon DL, Yoshioka T. Biophys. J. 1998; 74:82–89. [PubMed: 9449312]
20. Maciel GS, Alencar M, rcio ARC, de A, jo CB, Patra A. J. Nanosci. Nanotechnol. 2010; 10:2143–2148. [PubMed: 20355643]

21. Reichardt C. Chem. Rev. 1994; 94:2319–2358.
22. Parker D. Coord. Chem. Rev. 2000; 205:109–130.
23. Bullen C, Mulvaney P. Langmuir. 2006; 22:3007–3013. [PubMed: 16548550]
24. Liu Y-S, Sun Y, Vernier PT, Liang C-H, Chong SYC, Gundersen MA. J. Phys. Chem. C. 2007; 111:2872–2878.
25. Kagan CR, Murray CB, Nirmal M, Bawendi MG. Phys. Rev. Lett. 1996; 76:1517–1520. [PubMed: 10061743]
26. Oyama K, Takabayashi M, Takei Y, Arai S, Takeoka S, Ishiwata S. i. Suzuki M. Lab on a Chip. 2012; 12:1591–1593. [PubMed: 22437040]
27. Wuister SF, de Mello Donegá C, Meijerink A. J. Phys. Chem. B. 2004; 108:17393–17397.
28. van Sark WGJHM, Frederix PLTM, Van den Heuvel DJ, Gerritsen HC, Bol AA, van Lingen JNJ, de Mello Donegá C, Meijerink A. J. Phys. Chem. B. 2001; 105:8281–8284.
29. Suyver JF, Kelly JJ, Meijerink A. J. Lumin. 2003; 104:187–196.
30. Chen H-Y, Maiti S, Nelson CA, Zhu X, Son DH. J. Phys. Chem. C. 2012; 116:23838–23843.
31. Yu WW, Peng X. Angew. Chem. Int. Ed. 2002; 41:2368–2371.
32. Yang Y, Chen O, Angerhofer A, Cao YC. J. Am. Chem. Soc. 2006; 128:12428–12429. [PubMed: 16984188]
33. Chen H-Y, Maiti S, Son DH. ACS Nano. 2011; 6:583–591. [PubMed: 22176684]
34. Chen D, Viswanatha R, Ong GL, Xie R, Balasubramaninan M, Peng X. J. Am. Chem. Soc. 2009; 131:9333–9339. [PubMed: 19566099]
35. Zheng J, Ji W, Wang X, Ikezawa M, Jing P, Liu X, Li H, Zhao J, Masumoto Y. J. Phys. Chem. C. 2010; 114:15331–15336.
36. Maestro LM, Rodríguez E. M. n. Rodríguez FS, la Cruz M. C. I.-d. Juarranz A, Naccache R, Vetrone F, Jaque D, Capobianco JA, Solé J. G. a. Nano Lett. 2010; 10:5109–5115.
37. Vetrone F, Naccache R, Zamarrón A, Juarranz de la Fuente A, Sanz-Rodríguez F, Martinez Maestro L, Martín Rodriguez E, Jaque D, García Solé J, Capobianco JA. ACS Nano. 2010; 4:3254–3258. [PubMed: 20441184]
38. Larsen BA, Deria P, Holt JM, Stanton IN, Heben MJ, Therien MJ, Blackburn JL. J. Am. Chem. Soc. 2012; 134:12485–12491. [PubMed: 22746552]
39. Williams KJ, Tisdale WA, Leschkies KS, Haugstad G, Norris DJ, Aydil ES, Zhu XY. ACS Nano. 2009; 3:1532–1538. [PubMed: 19456114]
40. Law M, Luther JM, Song Q, Hughes BK, Perkins CL, Nozik AJ. J. Am. Chem. Soc. 2008; 130:5974–5985. [PubMed: 18396872]
41. Koo C, Godley RF, Park J, McDougall MP, Wright SM, Han A. Lab on a Chip. 2011; 11:2197–2203. [PubMed: 21603723]

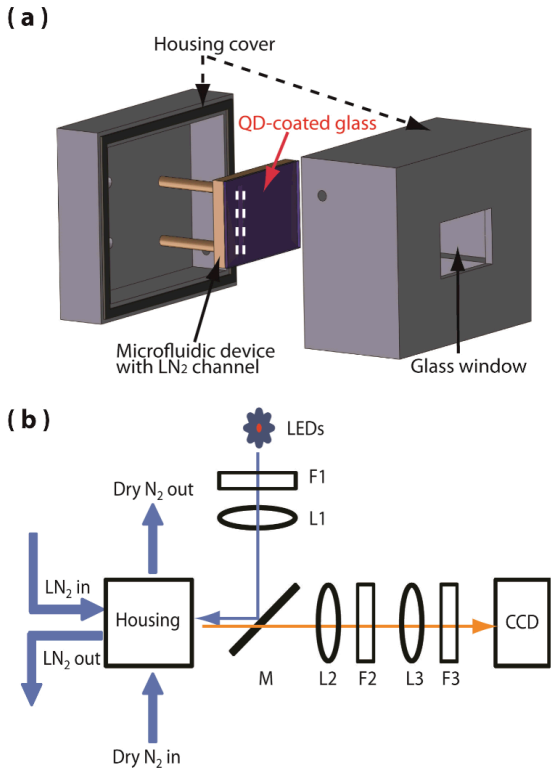

Fig. 1.

Schematics of the cryo-cooling device, the enclosure and the temperature measurement setup. (a) The cryo-cooling device is in the enclosure in which dry nitrogen is constantly flushed. (b) The optical setup consists of filters (F), achromatic doublet lenses (L), and a dichroic mirror (M). The device was illuminated with a 365 nm LED and imaged with a CCD detector.

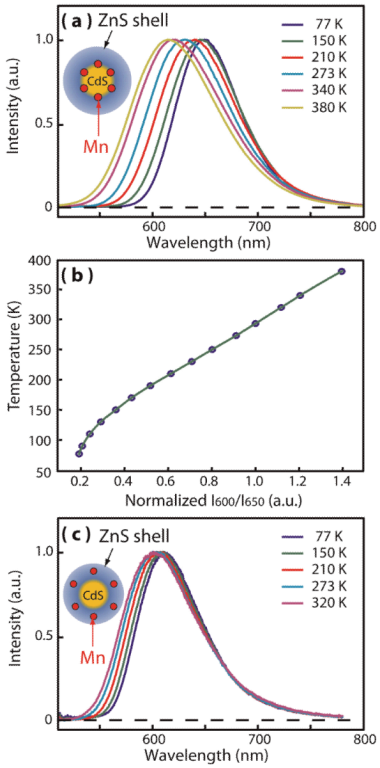

Fig. 2.

(a) Normalized Mn luminescence spectra of Mn-doped (at the interface between the CdS core and ZnS shell) NCs with high local lattice strain at Mn^{2+} sites used for thermometry in this study. (b) Intensity ratio of I_{600}/I_{650} at different temperatures (blue dots: experimental data, green line: interpolation curve). (c) Normalized Mn luminescence spectra of typical Mn-doped (in the ZnS shell) NCs with weak local lattice strain at Mn^{2+} ion sites. Insets in (a) and (c) pictorially represent the structures of Mn-doped core/shell NCs with different radial doping locations.

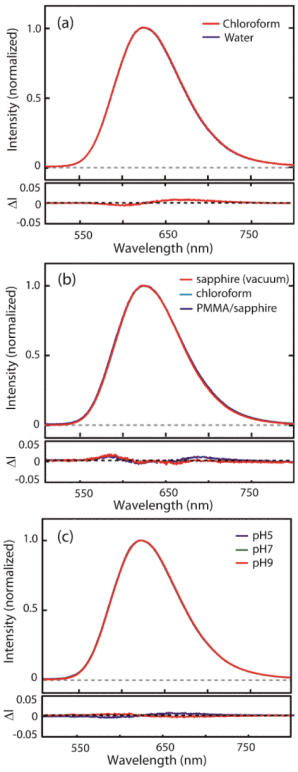

Fig. 3.

Comparison of the normalized luminescence spectra of Mn-doped CdS/ZnS NCs under different medium environment. (a) Solvent dependence; chloroform (s_1) and water (s_2), (b) Medium phase dependence; on sapphire under vacuum (s_3), PMMA/sapphire (s_4), chloroform (s_1) is shown for comparison. (c) pH dependence: pH5 (s_5), pH7 (s_6) and pH9 (s_7). The bottom panels are the intensity difference of the normalized spectra. (a) s_1–s_2, (b) s_1–s_3 (blue), s_1–s_4 (red), (c) s_6–s_5 (blue), s_6–s_7 (red).

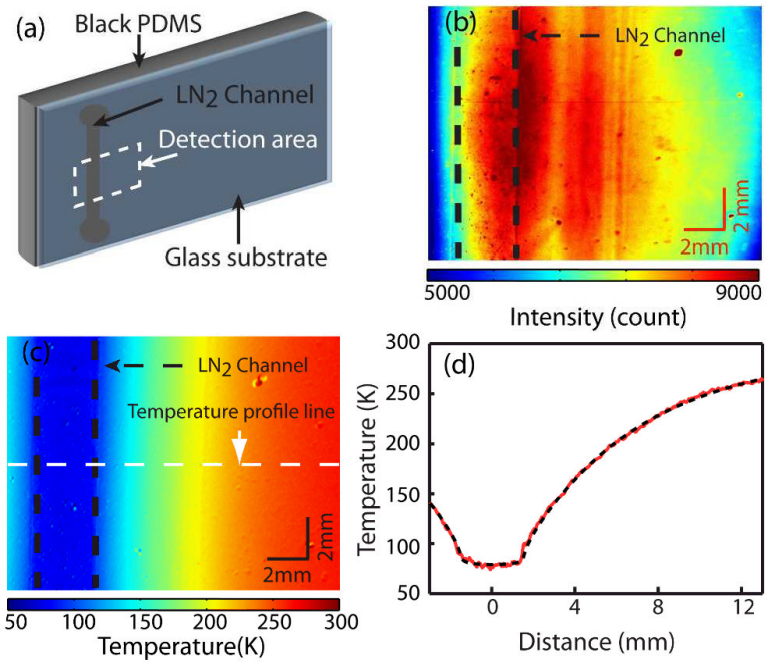

Fig. 4.

(a) Schematics of the cryo-cooling device. The imaging area is indicated by the dashed rectangle. (b) Color contour plot of the intensity 25 image (I_{650}) from the device with liquid nitrogen flow in the channel. (c) Color contour plot of the temperature converted from the intensity ratio image. (d) Temperature line profile (solid) and the simulation result (dashed) at the location indicated in (c).

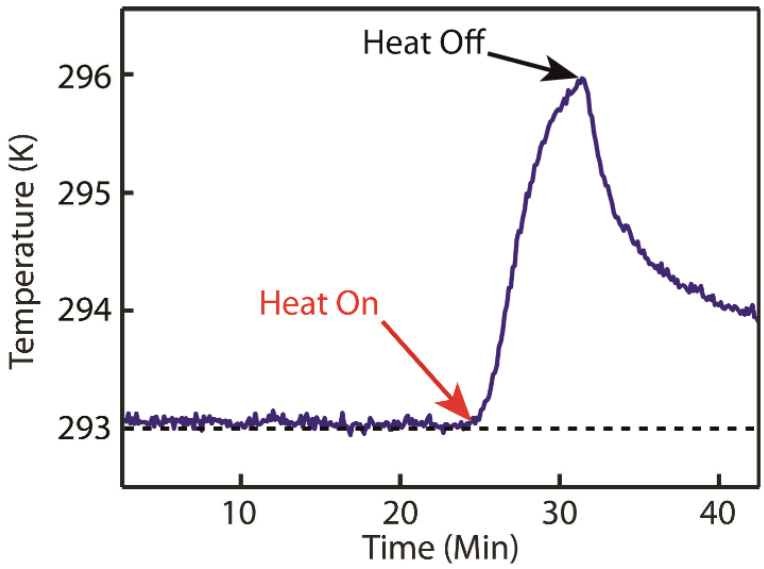

Fig. 5.

The time-profile of the temperature of hexane solution of the NCs in a cuvette under the constant and varying temperature conditions. The temperature trace is converted from the luminescence intensity ratio shown in Fig. 2(b).